Preliminary Study of Masonry – RC Hybrid Structure Behavior under Earthquake Loading

Y. Ouyang, H.J. Pam & S.H. Lo
The University of Hong Kong, Hong Kong, China

Y.L. Wong
The Hong Kong Polytechnic University, Hong Kong, China

J. Li
South China University of Technology, Guangzhou, China

ABSTRACT:
Low-rise confined masonry structures are widely used in earthquake-risked rural areas.   Most of these structures fail in shear pattern under lateral earthquake loading.   In this study, as an improvement for earthquake resistance and post-quake restoration, a masonry – reinforced concrete (RC) hybrid structure, whose working mechanism is different from that of its predecessor, is proposed.   The "tie beams" and 'tie columns", which function only as confinement in a conventional confined masonry wall structure, now also resist most of the gravity loading, while the wall panels take the rest of it.   On the other hand, wall panels in the proposed hybrid structure will absorb most of the energy induced by lateral earthquake loading by the formation of a plastic hinge region in the panel center so that severe damages can be controlled within the wall panel region.   To investigate shear behaviors of masonry walls, diagonal compression tests were performed and finite element simulation was utilized to verify the work mechanism of this hybrid structure.

Keywords: confined masonry wall, hybrid concrete-masonry wall, shear behavior.

1. INTRODUCTION

It has been a long history since our ancestors started to use masonry as one of construction materials, and nowadays people can still witness the marvel and splendor of masonry heritage from old times, e.g. the Great Wall of China, many prestigious castles in Europe etc.   Modern masonry buildings are commonly seen, however, in under-developed regions such as Mexico, South and Central America, and Middle East (Riahi et al. 2009), as well as in some rural areas of Europe and USA.   Compared with other construction materials like concrete and steel, masonry is economical in cost but inferior in mechanical properties.   Therefore, masonry is widely adopted only for low-rise construction in these regions.   However, some of these regions are considered as seismic-prone regions.   The low lateral resistance of plain masonry could not sustain even a moderate earthquake impact.   Therefore, many new techniques have been developed to enhance the earthquake performance of plain masonry structures.   Among them is the "confined masonry" (CM) method, which provides confining reinforced concrete (RC) members at the periphery of masonry panels.

As has been proven by experimental tests, CM structures are characterized with greater lateral strength and, more importantly, much higher ductility than plain masonry structures (Tomazevic and Klemenc 1997).   However, in CM systems the majority of gravity and seismic loads are resisted by the masonry panel, which is usually of low workmanship and lacks quality control during construction, thus yielding lower mechanical capacities than those tested in laboratory (Alcocer et al. 2003).

Therefore, the authors try to revise the CM system into a new form in that the RC members, which have better workmanship and quality control, will resist most of the gravity loads and the masonry panels will resist most of the earthquake loads.   The objectives of this proposed mechanism are: (1) to control the most severe damage within the masonry panel so that a plastic hinge will form therein; (2) to make sure that RC elements suffer limited damage during a moderate earthquake, so that the skeletal RC frame will remain intact after the event; and (3) to make it possible aftermath to restore the whole structure by repairing the damaged RC elements and replacing the damaged masonry panels.

This structural system is named masonry – RC hybrid wall (HBW) hereafter in this paper. The transfer of gravity load to RC members can be achieved by deliberately enlarging dimensions of the RC members and/or using higher grade concrete. A stiffer RC beam can help transfer most of the gravity load onto the RC columns rather than to the masonry panel below the beam, so that there will be less vertical stress in the masonry panel to enhance its lateral resistance as suggested by different models (Matsumura 1988, Moroni et al. 1994, Marinilli and Castilla 2006, Riahi et al. 2009).

Preliminary study of finite element simulation by Abaqus 6.11 software (Dassault Systèmes Simulia Corporation 2011) was carried out in this paper. A series of tests was conducted on two types of masonry (red and concrete bricks) assemblages to obtain their mechanical properties.

2. TEST PROGRAM

2.1. Pre-test Issues and Compressive Tests on Cement Mortars

Two types (red brick and concrete brick) of masonry specimens were tested to determine their basic mechanical properties, which were needed in the numerical simulation. The red bricks and concrete bricks have nominal dimensions of 210×99×55 and 220×97×65 mm respectively. To conform to the common practice of masonry construction, a mortar mix of 1/3.5/5.8 (water/cement/sand) by weight was adopted. Both types of bricks were soaked before being laid, and this would change the actual water content of mortar joints. Compressive strengths of the masonry specimens (f_m) were determined according to ASTM C 1314-07 "Test Method for Compressive Strength of Masonry Prisms" (ASTM International's Committee 2008), and diagonal compression tests were also conducted based on the provisions of ASTM E 519-07 "Test Method for Diagonal Tension (Shear) in Masonry Assemblages" (ASTM International's Committee 2008).

To monitor the strength of hand-mixed cement mortar (f_{cm}), twelve 50-mm mortar cubes were produced and tested according to ASTM C 107 "Test Method for Compressive Strength of Hydraulic Cement Mortars" (ASTM International's Committee 2008). Six of the specimens (CA1 to CA6) were cast on the same day and the rest (CB1 to CB3 and CC1 to CC3) were cast in two groups on two different days. The values of f_{cm} are listed in Table 1, together with the corresponding Young's modulus (E_{cm}) and Poisson's ratio (ν_{cm}) in the elastic range of these mortar specimens.

Table 1. Properties of mortar obtained in tests

Specimen code	Compressive strength f_{cm} (MPa)	Young's modulus E_{cm} (GPa)	Poisson's ratio ν_{cm}
CA1	47.4	2.54	0.061
CA2	46.6	3.53	0.085
CA3	51.2	3.91	0.083
CA4	30.1	1.64	0.045
CA5	31.6	1.99	0.062
CA6	33.6	2.97	0.057
CB1	38.9	2.43	0.047
CB2	34.2	3.28	0.073
CB3	32.0	2.81	0.041
CC1	33.7	2.69	0.055
CC2	33.0	2.74	0.065
CC3	31.9	3.38	0.074
Average value	37.0	2.83	0.063
Average value (without CA 1-3)	33.2	2.66	0.058
Standard deviation	7.0	0.62	0.014
Standard deviation (without CA 1-3)	2.0	0.46	0.010
*Coefficient of variation	18.8%	21.9%	22.0%
*Coefficient of variation (without CA 1-3)	6.2%	17.4%	16.9%

*Coefficient of variation = standard deviation / average value

In Table 1, specimens CA1 to CA3 have generally greater values in all the three parameters, and this causes high standard deviations and coefficients of variation. If specimens CA1 to CA3 are excluded, the standard deviations and coefficients of variations reduce considerably. Since specimens CA1 to CA3 were extracted from the same mixture of cement mortar as specimens CA4 to CA6, the large difference in compressive strength values indicates that the hand mixing practice of cement mortar in masonry construction can result in a very non-uniform mixture, which will conceivably impair the structural capacities due to occurrence of random planes of weakness. The large deviation of experimental results in E_{cm} is another evidence for non-uniform mixture, while that of v_{cm} can be attributed partly to the test set-up, since 50mm cube is of small dimension and thus very sensitive to minute discrepancies in strain gage locations.

2.2. Compression Tests on Masonry Prisms

Compression tests were conducted on four groups of masonry assemblages to obtain the compressive strength of masonry prisms. Each group consisted of three specimens affiliated to a particular wall specimen, as described in Table 2. Each specimen was composed of five stack brick units bonded by mortar joints with nominal thickness of 10 mm. The specimens were capped by plaster on both ends to facilitate loading. The compressive strength (f_m) of each prism is obtained by multiplying its failure stress with corresponding correction factor (see Table 3), which is dependent on the height/thickness ratio (h_p/t_p) of that prism (ASTM C 1314-07, ASTM International's Committee 2008). Failure modes of all the prisms were obtained by matching "Sketches of Mode of Failure" according to ASTM C 1314-07 (ASTM International's Committee 2008).

Table 2. Compressive strengths of masonry prisms

Affiliation to wall panel	Specimen code	Max. load (kN)	Failure stress (MPa)	h_p/t_p ratio	Correction factor	Failure mode	Compressive strength f_m (MPa)
	MP-A1	323.0	15.42	3.35	1.098	Face shell separation	
RW-A	MP-A2	343.4	16.93	3.40	1.102	Face shell separation	19.04
	MP-A3	407.1	19.67	3.31	1.095	Semi-conical break	
	MP-C1	460.0	22.35	3.72	1.098	Semi-conical break	
RW-B	MP-C2	420.0	20.05	3.76	1.090	Semi-conical break	22.71
	MP-C3	418.0	19.95	3.70	1.090	Face shell separation	
	MP-B1	105.0	4.90	3.35	1.127	Conical break	
CW-A	MP-B2	117.0	5.49	3.26	1.131	Cone & split	5.06
	MP-B3	67.0	3.08	3.25	1.126	Face shell separation	
	MP-D1	95.0	4.24	3.73	1.129	Cone & split	
CW-B	MP-D2	94.5	4.41	3.70	1.126	Face shell separation	4.87
	MP-D3	93.5	4.31	3.74	1.130	Face shell separation	

Table 3. Correction factors

h_p/t_p	1.3	1.5	2.0	2.5	3.0	4.0	5.0
Correction factor	0.75	0.86	1.0	1.04	1.07	1.15	1.22

As shown in Fig. 1, tensile splitting with vertical failure planes (i.e. face shell separation) and shear-tension with inclined failure planes (i.e. semi-conical / conical break) were the most commonly observed failure modes. Meanwhile, their failure combination (cone & split) occurred in two of the specimens. The failure modes are consistent with the previous finding, in which compressive failure of short stack-bonded prism is influenced by lateral tensile stress induced by differences in Young's moduli and Poisson's ratios between brick units and mortar joints (Francis et al. 1971).

| (a) Face shell separation | (b) Semi-conical / conical break | (c) Cone & split |

Figure 1. Different failure modes of masonry prisms

2.3. Diagonal Compression Tests

Single-layer masonry panels with nominal dimensions of 1200×1200×99 mm for the RW specimens and 1200×1200×97 mm for the CW specimens were fabricated. For each type of bricks (red and concrete bricks), two wall panels were produced, i.e. RW-A & RW-B of red bricks and CW-A & CW-B of concrete bricks. The RW and CW specimens consisted of respectively 20 and 17 layers of brick units with nominal thickness of bed joints controlled around 5 mm.
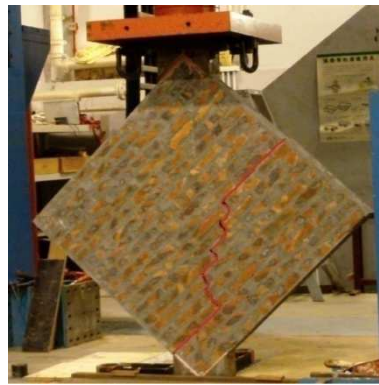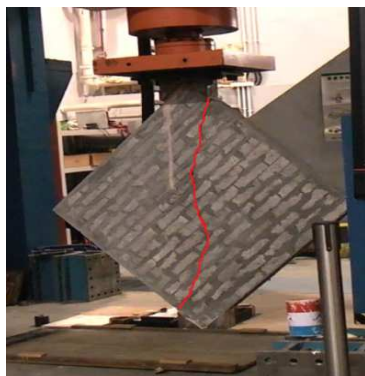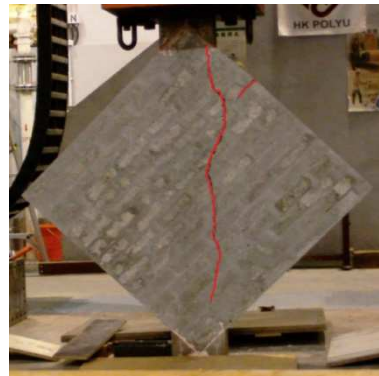
| (a) RW-A | (b) RW-B |

| (c) CW-A | (d) CW-B |

Figure 2. Diagonal compression tests

The diagonal compression test of each wall specimen was conducted beyond 28 days after fabrication. Each of the wall specimens was loaded in diagonal standing position via a pair of loading brackets, placed respectively on the top and at the bottom corners of the wall panel, as shown in Fig. 2.

Compressive diagonal load was applied gradually by a servo hydraulic jack (see Fig. 2), and the load magnitude at failure (P_d) was recorded.   The average shear ($\overline{\tau}$) can then be calculated using Eqn. 1, i.e.

$$\overline{\tau} = 0.707 \frac{P_d}{bt} \tag{1}$$

where b (1200 mm) is the height or length and t (99 and 97 mm for respectively the RW and CW specimens) is the thickness of the specimen.

By assuming the masonry as an isotropic homogeneous material, the highest value of maximum principal stress under diagonal compression, i.e. $\sigma_1 = 0.7336\overline{\tau}$ (positive for tension), is located at the geometrical center of the square panel, and its direction is along the horizontal diagonal (Frocht 1931). In fact, the critical maximum principal stress at any horizontal line occurs on the point of the vertical diagonal, and its direction is always horizontal for tension.   This explains diagonal splitting is the perfect pattern of failure for the above experimental set-up.   Although Frocht's (1931) stress distribution model for diagonal compression can be influenced by different assumed values of Poisson's ratio, the effect is so insignificant that can be ignored (Yokel and Fattal 1976).   Frocht (1931) adopted the value of minimum principal stress at the center, $\sigma_3 = -2.38\overline{\tau}$ (Frocht 1931).

According to Yokel and Fattal (1976), the uniaxial tensile strength of masonry wall specimens (f_t), as expressed by stress state $(0, f_t)$, can be obtained by linear extrapolation of two points on the $\sigma_1 - \sigma_3$ plane, i.e. $(f_m, 0)$ and $(-2.38\overline{\tau}, 0.7336\overline{\tau})$ (see Fig. 3).   The straight line connecting these three points is defined as the failure envelope of masonry assemblages.   The expression for f_t is

$$f_t = 0.7336\overline{\tau} \frac{f_m}{f_m + 2.38\overline{\tau}} \quad \text{where} \quad f_m < 0 \tag{2}$$
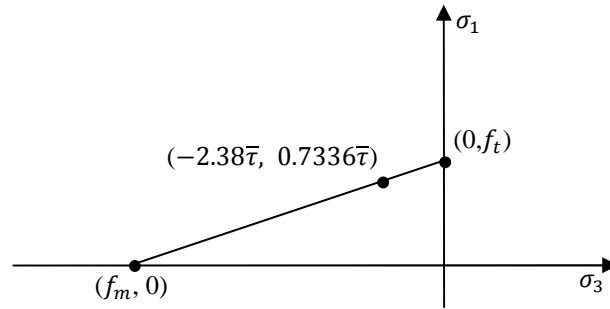

Figure 3. Yokel and Fattal's linear failure envelope (1976)

The experimental data in Table 4 and Fig. 4 show that although the RW specimens possess higher shear ($\overline{\tau}$) and compressive strengths (f_m), the CW counterparts have higher ductility and energy absorption, which are the most important characteristics for seismic performance evaluation.

Table 4. Experimental data from diagonal compression tests

| Wall specimen	P_d (kN)	$\overline{\tau}$ (MPa)	f_m (MPa)	f_t (MPa)	Energy absorption (J)
RW-A	279.0	1.66	19.04	1.54	376.6
RW-B	162.0	0.96	22.71	0.79	130.0
Average of red brick masonry		1.31	20.88	1.16	253.3
CW-A	168.0	1.02	5.06	1.44	241.1
CW-B	208.5	1.27	4.87	2.44	413.0
Average of concrete brick masonry		1.14	4.97	1.94	326.1
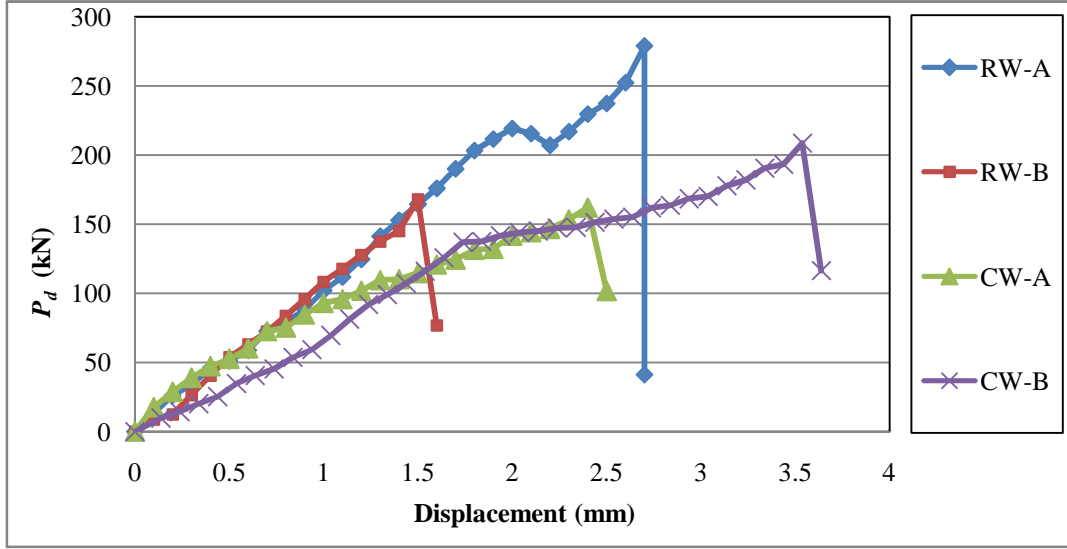
Figure 4. Measured load-displacement curves for wall specimens

However, in actual experimental tests, failure does not always initiate from the center and propagate along the vertical diagonal. Different failure modes were observed in the RW and CW specimens, as highlighted in Fig. 2. From Figs. 2a and 2b, it is obvious that the main cracks tend to develop along the mortar joints and not along the diagonal as expected in the RW specimens. This non-preferred failure pattern in the RW specimens is caused by excessive strength of the red bricks, so that sliding shear failure prevails and cracks seldom penetrate through the brick units. On the other hand, as shown in Figs. 2c and 2d, the failure pattern of the CW specimens is much closer to the ideal pattern, in which the main cracks occurred almost along the vertical diagonal direction passing both concrete brick units and mortar joints.

The different failure patterns in the RW and CW specimens explained above are correlated with the degree of heterogeneity in masonry structures. From the sliding shear failure observed in the RW specimens, one can come up with a reasonable deduction that the tensile strength obtained from the diagonal compression tests reflects the bond strength between the mortar joints and the red brick units, or tensile and shear strength of the mortar itself. These strengths can be taken as the failure limits in assessing the shear-tension capacity of the more heterogeneous masonry walls (Abdelkrim et al. 2008), such as the RW specimens. As for the CW specimens, due to the rough texture of the concrete brick surfaces, bond strength is sufficient enough not to become the failure limit.

2.4. Numerical Simulation

2.4.1. Numerical simulation on the CW diagonal compression tests
As discussed before, the CW walls have better ductility and energy absorption capacities than those of the RW walls, so it is reasonable to numerically construct the HBW by using concrete brick units instead of red bricks. Since CW walls have exhibited sufficient homogeneity in the previous diagonal compression tests, their brick units and mortar do not have to be modeled separately. Mander's unconfined compressive stress-strain model (Mander et al. 1988) and Sima's cracking model (Sima et al. 2008) are adopted to obtain respectively compressive stress σ_c and tensile stress σ_t at any strain ε, i.e.

$$\sigma_c = \frac{f_c \, x \, r}{r - 1 + x^r} \tag{3}$$

$$\sigma_t = \begin{cases} E_o \varepsilon & \text{for} \quad \varepsilon \leq \varepsilon_{ct} \\ E_o \varepsilon_{ct} e^{\alpha\left(1 - \frac{\varepsilon}{\varepsilon_{ct}}\right)} & \text{for} \quad \varepsilon > \varepsilon_{ct} \end{cases} \tag{4}$$

where f_c is compressive strength, taken as f_m for specimens CW-A and CW-B; $x=\varepsilon/\varepsilon_{co}$; ε_{co} is the strain corresponding to f_c, normally taken as 0.002; $r=E_o/(E_o-E_{sec})$; E_o is initial Young's modulus; $E_{sec}=f_c/\varepsilon_{co}$; $\varepsilon_{ct}=f_{ct}/E_o$ is initial cracking strain; f_{ct} is tensile strength, taken as f_t obtained from the diagonal compression tests; $\alpha=[G_f E_o/(l^* f_{ct}^2)-0.5]^{-1}\geq0$; G_f is fracture energy, taken as 40 J/m^2; l^* is characteristic length, taken as 0.0035. Although it is suggested that theoretically $E_o = 1000f_c$ for masonry in Eurocode 6 (CEN 1995), the actual E_o varies from $200f_m$ to $2000f_m$ (Tomazevic 1999). For the CW walls studied in this paper, it is assumed that $E_o = 550f_m$. The numerical simulation results by Abaqus (Dassault Systèmes Simulia Corporation 2011) for specimens CW-A and CW-B are shown in Fig. 5 together with the experimental counterparts. It is seen from the figure that the ratios of theoretical over experimental ultimate loads for specimens CW-A and CW-B are 1.10 and 0.84 respectively.
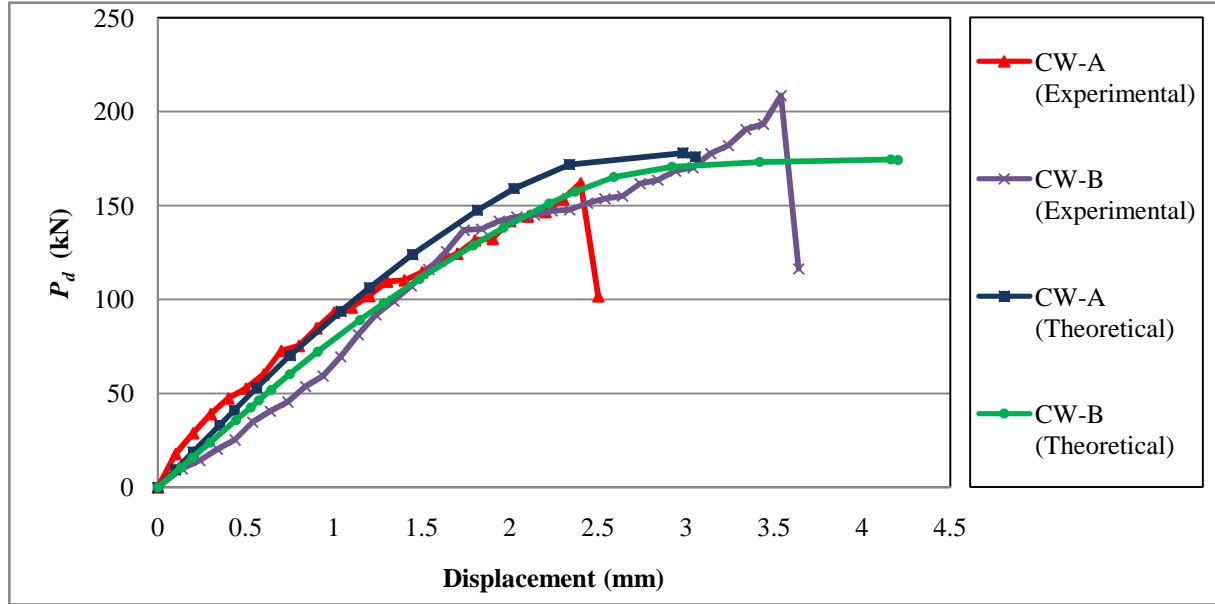

Figure 5. Numerical simulation results for CW-A and CW-B by Abaqus

2.4.2. Numerical simulation on HBW structure

As the model can closely define the behavior of concrete brick masonry, a numerical simulation to validate the feasibility of the proposed HBW subjected to lateral loading (simulating earthquake) is carried out. The RC members (beam and columns) contain concrete of 30 MPa cube strength (f_{cu}) and reinforcement steel of 460 MPa yield strength (f_y). An elasto-plastic bilinear model is adopted for the steel reinforcement with Young's modulus set to be 200 GPa. The above Mander's (1988) and Sima's (2008) analytical models are applied to concrete and masonry. For the concrete, the initial Young's modulus $E_o=3.46\sqrt{f_{cu}}+3.21$ (in GPa), based on Hong Kong Code of Practice for Structural Use of Concrete (Buildings Department 2004); the compressive strength $f_c=0.8f_{cu}$; the tensile strength $f_{ct}=0.08f_{cu}$; and the fracture energy $G_f=100$ J/m^2. For the masonry, f_c and f_{ct} are taken as the average of respectively f_m and f_t of the CW specimens; $E_o=550f_m$ and $G_f=40$ J/m^2. For both concrete and masonry models, ε_{co} and l^* are considered as 0.002 and 0.0035 respectively. The concrete columns have cross-section dimensions of 180×180 mm and longitudinal steel ratio of 5.8%; the concrete beam has cross-section dimensions of 140×180 mm (breadth×depth) and longitudinal steel ratio of 1.8%; and the masonry panel has dimensions of 2200×2200×97 mm. Monotonic lateral loading (push-over) simulating earthquake effect was applied, as shown in Fig. 6.

Maximum and minimum in-plane principal plastic strain (PE) contour diagrams at the maximum lateral loading with the drift ratio of 0.13% were obtained from the numerical simulation (Figs. 6a and 6b). Given that reversed loading generates mirrored contours about the axis of symmetry, the center of wall panel will become further plastically strained under earthquake loading. Therefore, plastic hinge will most likely occur at the center of the masonry panel. It is worth noting that the beam-masonry and column-masonry interfaces may detach during earthquake attacks, thus special

detailing is needed to avoid premature failure at those locations.

| (a) Maximum principal plastic strain | (b) Minimum principal plastic strain |
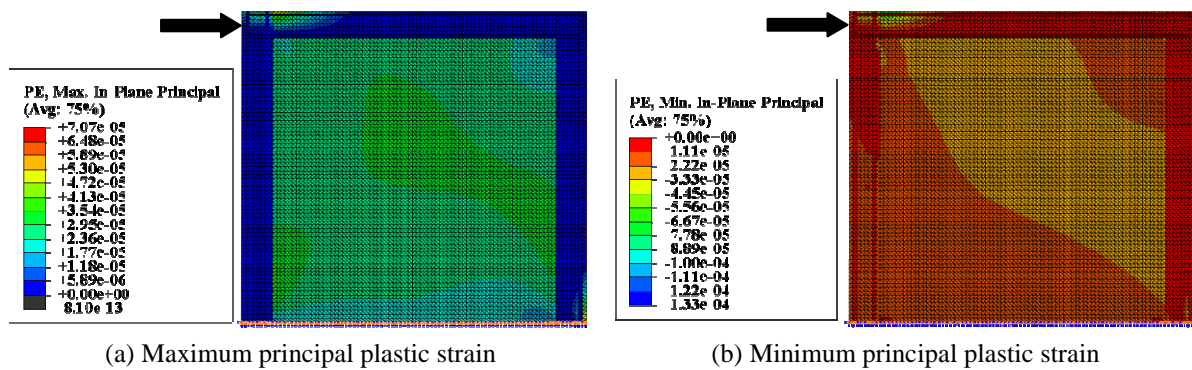
Figure 6. Strain contours of HBW structure under simulated earthquake loading

3. CONCLUSIONS

From the diagonal compression tests of red-brick (RW specimens) and concrete-brick (CW specimens) wall panels, it is obvious that the latter is more ductile. The crack pattern in the CW specimens developed along the diagonal and passed through the brick units. However, failure in the RW specimens happened along the mortar joints in a form of sliding shear failure, which is not preferred. Therefore, concrete bricks are more suitable for HBW in resisting earthquake loading.

From the numerical simulation, it is exhibited that HBW structures with major plastic hinge formed at the center of the wall panel under earthquake loading is feasible as long as sufficient strength and ductility are provided in the concrete frames. In addition, to avoid occurrence of weak planes along mortar joints and achieve diagonal cracking failure pattern instead of sliding failure, a better quality control on cement mortar is required and more ductile brick units (e.g. concrete bricks) are proposed to be used.

To further control the occurrence of plastic hinge within the center of wall panel, anchorage acting as stiffeners in the form of reinforcing steel bars is proposed to be installed along the masonry-concrete interface, so that the peripheral of the wall panel is strengthened. Further experimental tests are needed to examine the effect of this peripheral stiffener in HBW under monotonic and/or reversed cyclic earthquake loading.

REFERENCES

Abdelkrim B., Tetsuro G. and Masakatsu M. (2008). Shear capacity prediction of confined masonry walls subjected to cyclic lateral loading. *Structural Engineering/Earthquake Engineering,* 25:2, 47-59.

Alcocer S.M., Cesin J., Flores L.E., Hernandez O., Meli R., Tena A. and Vasconcelos D. (2003). The New Mexico City code requirements for design and construction of masonry structures. *9th North American Masonry Conference.* EUA, Clemson, S.C.: 656-667.

ASTM International's Committee C12 & C15 (2008). ASTM Masonry Standards for the Building Industry, 6th Edition, ASTM International, West Conshohocken, PA, USA.

Buildings Department (2004). Code of Practice for Structural Use of Concrete. Buildings Department, The Government of the Hong Kong S.A.R.

CEN (1995). Eurocode 6: Design of masonry structures, Part 1-1: General rules for buildings. Rules for reinforced and unreinforced masonry. ENV 1996-1-1: 1995.

Dassault Systèmes Simulia Corporation (2011). Abaqus User Manual Version 6.11.

Francis A.J., Horman C.B. and Jerrems L.E. (1971). The effect of joint thickness and other factors on the compressive strength of brickwork. *Proceedings of the Second International Brick Masonry Conference*, British Ceramic Research Association, Stoke-on-Trent, UK, 31-37.

Frocht M.M. (1931). Recent Advances in Photoelasticity, *Transactions*, ASM, 55, Sep.-Dec. 1931, 135-153.

Mander J.B., Priestley M.J.N. and Park R. (1988). "Theoretical stress-strain model for confined concrete", *Journal of Structural Engineering*, ASCE, 114:8, 1805-1826.

Marinilli A. and Castilla E. (2006). Seismic behavior of confined masonry walls with intermediate confining-columns. *8th U.S. National Conference on Earthquake Engineering*. Proceeding: No. 607.

Matsumura A. (1988). Shear strength of reinforced masonry walls. *9th World Conference on Earthquake Engineering*. Proceeding: 121-126.

Moroni M.O., Astroza M. and Tavonatti S. (1994). Nonlinear models for shear failure in confined masonry walls. *Masonry Society Journal*. 12:2, 72-78.

Riahi Z., Elwood K.J. and Alcocer S.M. (2009). Backbone model for confined masonry walls for performance-based seismic design. *Journal of Structural Engineering*. 135:6, 644-654.

Sima J.F., Roca P. and Molins C. (2008). Cyclic constitutive model for concrete. *Engineering Strucutures*. 30:3, 695-706.

Tomazevic M. (1999). Earthquake resistant design of masonry buildings, London: Imperial College Press.

Tomazevic M. and Klemenc I. (1997). Seismic behavior of confined masonry walls. *Earthquake Engineering and Structural Dynamics*. 26:10, 1073-1088.

Yokel F.Y. and Fattal S.G. (1976). Failure hypothesis for masonry shear walls. *Journal of Structural Division, ASCE*, 102:3, 515-532.